Role of the crystalline form of titanium dioxide nanoparticles: Rutile, and not anatase, induces toxic effects in Balb/3T3 mouse fibroblasts

Uboldi, Chiara; Urbán, Patricia; Gilliland, Douglas; Bajak, Edyta; Valsami-Jones, Eugenia; Ponti, Jessica; Rossi, François

DOI:
10.1016/j.tiv.2015.11.005

Document Version
Peer reviewed version

Citation for published version (Harvard):
Uboldi, C, Urbán, P, Gilliland, D, Bajak, E, Valsami-jones, E, Ponti, J & Rossi, F 2016, 'Role of the crystalline form of titanium dioxide nanoparticles: Rutile, and not anatase, induces toxic effects in Balb/3T3 mouse fibroblasts', Toxicology in Vitro, vol. 31, pp. 137-145. https://doi.org/10.1016/j.tiv.2015.11.005

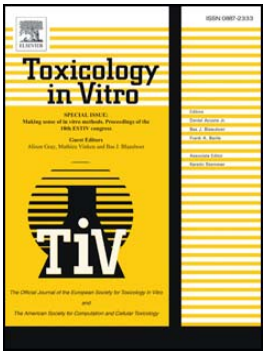

Role of the crystalline form of titanium dioxide nanoparticles: Rutile, and not anatase, induces toxic effects in Balb/3T3 mouse fibroblasts

Chiara Uboldi, Patricia Urbán, Douglas Gilliland, Edyta Bajak, Eugenia Valsami-Jones, Jessica Ponti, François Rossi

PII: S0887-2333(15)30006-0
DOI: doi: 10.1016/j.tiv.2015.11.005
Reference: TIV 3664

To appear in:

Received date: 18 May 2015
Revised date: 23 September 2015
Accepted date: 9 November 2015

Please cite this article as: Uboldi, Chiara, Urbán, Patricia, Gilliland, Douglas, Bajak, Edyta, Valsami-Jones, Eugenia, Ponti, Jessica, Rossi, François, Role of the crystalline form of titanium dioxide nanoparticles: Rutile, and not anatase, induces toxic effects in Balb/3T3 mouse fibroblasts, (2015), doi: 10.1016/j.tiv.2015.11.005

Role of the crystalline form of titanium dioxide nanoparticles: rutile, and not anatase, induce toxic effects in Balb/3T3 mouse fibroblasts

Chiara Uboldi [a], Patricia Urbán [a], Douglas Gilliland [a], Edyta Bajak [a], Eugenia Valsami-Jones [b,c], Jessica Ponti [a*] and François Rossi [a]

[a] European Commission, Joint Research Centre, Institute for Health and Consumer Protection, NanoBioSciences Unit, Ispra (VA), Italy
[b] Natural History Museum, Department of Earth Sciences, London SW7 5BD, UK
[c] University of Birmingham, School of Geography, Earth and Environmental Sciences, Birmingham B15 2TT, UK

chiara.uboldi@imbe.fr

patricia.urban-lopez@ec.europa.eu

douglas.gilliland@ec.europa.eu

eda_adenov@yahoo.com

e.valsamijones@bham.ac.uk

jessica.ponti@ec.europa.eu

francois.rossi@ec.europa.eu

*Corresponding author: Jessica Ponti, Joint Research Centre, IHCP, NBS Unit, TP203, via E. Fermi 2749, 21027 Ispra, (VA), Italy. Tel. +39 0332 785793; Fax: +39 0332 785787; e-mail: jessica.ponti@ec.europa.eu

Abstract

The wide use of titanium dioxide nanoparticles (TiO_2 NPs) in industrial applications requires the investigation of their effects on human health. In this context, we investigated the effects of nanosized and bulk titania in two different crystalline forms (anatase and rutile) *in vitro*. By colony forming efficiency assay, a dose-dependent reduction of the clonogenic activity of Balb/3T3 mouse fibroblasts was detected in the presence of rutile, but not in the case of anatase NPs. Similarly, the cell transformation assay and the micronucleus test showed that rutile TiO_2 NPs were able to induce type-III foci formation in Balb/3T3 cells and appeared to be slightly genotoxic, whereas anatase TiO_2 NPs did not induce any significant neoplastic or genotoxic effect. Additionally, we investigated the interaction of TiO_2 NPs with Balb/3T3 cells and quantified the *in vitro* uptake of titania using mass spectrometry. Results showed that the internalization was independent of the crystalline form of TiO_2 NPs but size-dependent, as nano-titania were taken up more than their respective bulk materials.

In conclusion, we demonstrated that the cytotoxic, neoplastic and genotoxic effects triggered in Balb/3T3 cells by TiO_2 NPs depend on the crystalline form of the nanomaterial, whereas the internalization is regulated by the particles size.

Keywords: titanium dioxide nanoparticles; cytotoxicity; morphological neoplastic transformation; genotoxicity; micronucleus; uptake

Introduction

Titanium dioxide nanoparticles (TiO_2 NPs, titania) are currently used in a variety of applications ranging from the paper industry, where they confer whiteness and opacity in cellulose papers (Huang *et al*., 2011), to the production of antifogging and self-cleaning glasses and plastics (Howarter and Youngblood, 2008). TiO_2 NPs are also used as food color additives and flavor enhancers (Weir *et a*l. 2012) and in various cosmetics owing to their ability to absorb and scatter UV light (Wolf *et al*. 2003; Shi *et al*. 2013). Due to their photocatalytical properties titania can additionally be employed in the degradation of pollutants in water treatment implants (Chong *et al*. 2010).

Nevertheless, the wide use of TiO_2 NPs, which naturally can occur in three different crystalline forms namely anatase, rutile and brookite, raised concern in the last years. Based on the evidence that titania can induce lung cancer in rats, the International Agency for Research on Cancer (2010) classified TiO_2 NPs as possibly carcinogenic to humans (group 2B). In fact, lung tumors (Xu *et al.*, 2010), broncho-alveolar adenomas and cystic keratinizing squamous cell carcinomas (Mohr *et al*. 2006) developed following inhalation and instillation of, respectively, rutile and anatase TiO_2 NPs.

In addition, nowadays several studies report that titania might be harmful to human health. Rutile titania impaired the viability of human amnion cells (Saquib *et al*., 2012), skin fibroblasts and human epidermoid carcinoma cells (Uchino *et al*., 2011), but cytotoxicity was observed also in Chinese hamster fibroblasts (Hamzeh and Sunahara, 2013). Similarly, anatase TiO_2 NPs induced oxidative stress, apoptosis and impairment of the mitochondrial activity in *in vitro* human-derived glial and lung cells (Aueviriyavit *et al*., 2012; Huerta-Garcia *et al*. 2014). Moreover, anatase exerted cytotoxic effects in Chinese hamster fibroblasts (Chen *et al*. 2014) and in murine

osteocells (Bernier *et al*., 2012; Di Virgilio *et al*., 2010b). However, anatase was not cytotoxic in human intestinal cells (De Angelis *et al.*, 2013), as well as in nasal mucosa cells (Hackenberg *et al.*, 2010) and in lymphocytes (Hackenberg *et al.*, 2011).

Analogously, no conclusive results on the genotoxic potential exerted *in vitro* by anatase and rutile NPs have been reported. Increased DNA strand breaks and chromosome aberrations were detected in human intestinal, amniotic and epidermal cells (Saquib *et al.*, 2012; Shukla *et al*., 2011), and in Chinese hamster ovary and lung fibroblasts exposed to the two types of titania (Di Virgilio *et al*., 2010; Hamzeh and Sunahara, 2013). Conversely, anatase TiO_2 NPs were not able to induce DNA damage in human nasal mucosa (Hackenberg *et al.*, 2010) and peripheral blood lymphocytes (Hackenberg *et al.*, 2011).

Although many studies have been published showing experimental evidences of the toxic potential of TiO_2 NPs, the role played by the crystalline form of titania in the toxic mechanisms is still unclear. In this study, we evaluated the effects induced *in vitro* by TiO_2 NPs in Balb/3T3 mouse fibroblasts which after exposure to carcinogens become tumourigenic forming morphologically transformed colonies (foci type III). Their ability to induce cancer *in vivo* is detectable by injecting the transformed cells in nude mice and observing their growth as sarcomas (Kurzepa *et al*., 1984; Saffiotti & Ahmed 1995). This cell model was selected among Syrian Hamster Embryo (SHE) cells, C3H10T1/2 and Bhas42 *in vitro* models (Kerckaert *et al*., 1996; Isfort & LeBoeuf, 1996; Balls & Clothier, 2010) alternative to the use of animals able to detect morphological neoplastic transformation potential induced by chemicals and nanomaterials (NM).

In particular, we compared the effects exerted by two crystalline forms (anatase and rutile) of nanosized titania with their respective bulk materials, focusing not only on the cytotoxicity and

the morphological transformation induced by TiO_2 NPs, but investigating also the genotoxicity of titania and their internalization in Balb/3T3 cells. The *in vitro* cytotoxicity was assayed performing the non-colorimetric Colony Forming Efficiency (CFE) test, while Cell Transformation Assay (CTA) evaluated morphological neoplastic transformation induced by anatase and rutile TiO_2 NPs. To investigate if TiO_2 NPs are able to induce chromosomal damage, we performed the cytokinesis-blocked micronucleus (CBMN) assay, and the uptake of titania in Balb/3T3 cells was investigated by Inductively Coupled Plasma-Mass Spectrometry (ICP-MS), which allowed us to perform a correlation between the amount (expressed as mass and number of particles) of TiO_2 NPs internalized and their toxic potential.

Materials and Methods

Synthesis and characterization of TiO_2 NPs

Pure anatase and rutile TiO_2 NPs were obtained by hydrolysis and oxidation of $TiCl_3$ as previously described (Cassaignon *et al*., 2007; Valsami-Jones *et al*., 2008; Sweeney *et al*. 2014). Stock suspensions of nanosized anatase (An-10), nanosized rutile (Ru-10), bulk anatase (BAN) and bulk rutile (BRU) were characterized in deionized water by Dynamic Light Scattering (DLS) and Transmission Electron Microscopy (TEM). For TEM analysis, each sample was dropped onto ultrathin Formvar-coated 200-mesh copper grids (Ted Pella, Inc.; USA) and left to air dry before image acquisition was performed with a JEOL 2100 electron microscope (JEOL USA, Inc.; USA). Zeta-potential was also recorded for all the samples at pH 7. To further investigate their behavior, TiO_2 NPs were characterized by centrifugal liquid sedimentation (CLS) in deionized water and at increasing time points (0 – 24 – 48 – 72 h) incubation in complete cell culture medium. Before each analysis stock suspensions of TiO_2 NPs were bath-sonicated (10

min) and then aliquots were added to deionized water or to complete cell culture medium to obtain 0.1 mg/ml test suspensions. CLS characterization was performed by using the DC24000UHR centrifugal particle sedimentation (CPS Instruments; The Netherlands) operated at a speed of 30,000 x g in an 8-24 % wt sucrose density gradient.

Cellular system

Immortalized Balb/3T3 mouse fibroblasts (clone A31-1-1) purchased from Hatano Research Institute (Japan). Cells were cultivated under normal cell culture conditions (37°C; 5% CO_2; 95% humidity) in complete cell culture medium composed of Modified Essential Medium (MEM) 1X (Invitrogen; Italy), supplemented with 10% (v/v) foetal bovine serum – Australian origin (Invitrogen; Italy) and 1% (v/v) antibiotics (Invitrogen; Italy). Sub-confluent cells (70-80 %) were passaged weekly in tissue culture-treated flasks (BD Falcon; Italy).

Colony Forming Efficiency (CFE) test

To investigate the potential *in vitro* cytotoxicity of TiO_2 NPs in Balb/3T3 mouse fibroblasts, Colony Forming Efficiency (CFE) assay was performed as previously described (Uboldi *et al.*, 2012). Deionized water and sodium chromate (1000 µM) were used as solvent (C solv) and positive (C +) control, respectively. After TiO_2 NPs were bath-sonicated for 10 min, aliquots of the stock suspensions were directly pipetted into the culture dishes to obtain the desired test concentrations (1 – 5 – 10 µg/ml) and cells were exposed to titania for 24 h and 72 h.
The number of colonies was scored using the software-operated colony counter GelCount™ (Oxford Optronix Ltd.; UK). Data were normalized to the solvent control and expressed as % CFE [(average of treatment colonies / average of solvent control colonies) × 100]. The standard

error of the mean (SEM) was calculated for 3 independent experiments and 3 replicates for each experimental point (SEM = standard deviation / square root of the number of replicates). Statistical significance was calculated by *one-way ANOVA* analysis with Bonferroni post hoc test (GraphPad Prism5 statistical software, GraphPad Inc.; USA).

Cytokinesis-blocked micronucleus (CBMN) test

To test the genotoxic potential of TiO_2 NPs, we performed the CBMN test as already described (Uboldi *et al.* 2012). Cells were exposed to the fixed concentration of 10 µg/ml for each TiO_2 NPs. The data (3 independent experiments and 3 replicates for each experiments performed) were analyzed by manually scoring the presence of micronuclei (MN) in 1000 binucleated (BN) cells. The results are expressed as the number of binucleated micronucleated (BNMN) cells per 1000 binucleated cells (BNMN/1000 BN cells) ± SEM. Statistical analysis was performed by *one-way* ANOVA with Bonferroni post hoc test (GraphPad Prism5 statistical software, GraphPad Inc.; USA), and differences versus C solv (ultrapure water) were considered statistically significant at $p < 0.05$.

Cell Transformation Assay (CTA)

Cell transformation assay (CTA) was performed to test if TiO_2 NPs can induce morphological neoplastic transformation in Balb/3T3 fibroblasts since they become tumourigenic forming morphologically transformed colonies (foci type III). CTA is considered a powerful tool to investigate *in vitro* the morphological neoplastic transformation induced by chemicals and nanomaterials (Vanparys *et al.*, 2010; Ponti *et al.*, 2013). Recently, its development into an OECD test guideline was recommended (EURL ECVAM, 2012).

As previously described (Uboldi *et al*., 2012; Ponti *et al.*, 2013), Balb/3T3 cells were seeded in 100 mm-Petri dishes ($3.34x10^3$ cells/ml; 6 ml/dish; 3 independent experiments and 5 replicates per concentration) and exposed for 72 h to TiO_2 NPs (Table 1). Untreated Balb/3T3 cells and cells exposed to 4 µg/ml of 3 - methylcholanthrene (Sigma-Aldrich; Italy) were used as negative and positive controls, respectively. After fixation (4% (v/v) of formaldehyde in PBS) and staining (10% (v/v) Giemsa solution in ultrapure water), the morphologically transformed colonies (type-III foci) were scored as described by the International Agency for Cancer research IARC Working-Group (IARC/NCI/EPA, 1985). Transformation results were expressed as transformation frequency (T_f) using the formula $T_f = [A/(B \times C \times D)]$, where A = total number of type III foci per treatment; B = CFE(%)/100; C = Plating Efficiency (%)/100; D = number of cell seeded multiplied per the number of plates; Plating Efficiency (%) = [(number of colonies formed in the control x 100) / 200], and 200 is the total number of cells initially seeded in each dish. Statistical analysis was performed applying the *F-Fisher exact test* and results were considered significant versus solvent control only when $p < 0.05$.

Uptake of TiO_2 NPs

To verify and quantify the uptake of TiO_2 NPs in Balb/3T3 mouse fibroblasts, the Inductively Coupled Plasma-Mass Spectrometry (ICP-MS) technique was perfomed using a 7700 series ICP-MS (Agilent Technologies Inc.; Italy). $5x10^5$ Balb/3T3 cells were seeded in 75 cm^2 tissue culture treated flasks (BD Falcon; Italy) in 10 ml of complete cell culture medium, and treated with a nominal concentration of 0.5 mg/ml TiO_2 NPs.

After 72 h exposure, the medium was collected for each test sample and stored at - 20°C. The cells were washed twice with 5 ml PBS, and each wash was collected in a separate tube and

frozen for further analysis. Balb/3T3 cells were trypsinized, suspended with 9 ml of complete culture medium and then counted using a TC10 automated cell counter (Bio-Rad; Italy). After centrifugation, the supernatant was collected into a new tube and the dried pellet stored at - 20°C. Before performing ICP-MS analysis, the frozen samples were restored at RT. To quantify the amount of Ti internalized, the cellular pellet was mineralized with Aqua Regia (HNO_3: HCl, 1:3 v/v) and digested in a microwave (Discover SP-D; CEM SRL; Italy). Two independent experiments (3 replicates each experiment) were carried out and results were expressed as picograms (pg) of uptaken Ti /cell using the formula *(A/B) x C*, where *A* = [Ti], expressed as ppb, at the end of the experiment; *B* = total number of cells at the end of the experiment and *C* = conversion factor ppb to pg. We also calculated the number of internalized TiO_2 NPs /cell using the formula *D/B*, where *D* = number of TiO_2 NPs at the end of the experiment. D was calculated transforming the concentration of titania found in the cellular pellet in mass of nanoparticles. This value was transformed into number of nanoparticles knowing that titania are insoluble (De Angelis et al., 2013) and assuming that most of the particles are spherical and well dispersed. Statistical analysis was performed applying t-test and results were considered significant when $p < 0.05$.

Results

Characterization of TiO_2 NPs: hydrodynamic diameter, PDI and Z-potential

DLS measurements (Table 1) showed that the mean size diameter of as-synthesized An-10 and Ru-10 was 51.42 ± 0.35 nm and 134.40 ± 1.02 nm respectively while it was 333.80 ± 2.90 nm and 734.20 ± 15.56 nm for BAN and BRU respectively. Polydispersity index (PDI) for these samples were ranging between 0.17 ± 0.01 and 0.24 ± 0.04, indicating that TiO_2 NPs were

relatively well dispersed in suspension. The Z-potential values at pH 7.0 for An-10 (- 5.64 ± 0.77 mV), Ru-10 (+ 0.04 ± 0.13 mV) and BRU (- 6.62 ± 3.90 mV) indicated a tendency to agglomerate/aggregate, whereas BAN resulted highly negative (- 48.40 ± 1.04 mV) and stable. TEM characterization (Figure 1) indicated that An-10 is composed by primary particles of ovoid and spherical shape with a mean size diameter ranging from 11 nm to 18 nm, while Ru-10 showed more elongated particles ranging from 10 nm to 35 nm. BAN and BRU were highly aggregated and composed of particles with different geometry, whose size ranged from 60 nm to 400 nm (BAN) and from 250 nm to 600 nm (BRU).

Further physico-chemical characterization of TiO_2 NPs suspensions (100 µg/ml) in deionized water and in cell culture medium supplemented with 10% serum was performed by CLS (Table 2). Freshly prepared An-10 (t = 0 h) resulted in nanoparticles of the same mean size range either in water or in culture medium (49 ± 21 nm and 46 ± 15 nm, respectively), while a slight but not significant increase in its hydrodynamic diameter was observed after 24 – 48 – 72 h incubation. Similarly, Ru-10 showed no significant increase in mean diameter when the value in water was compared to the particles size measured in the presence of serum proteins and at increasing time points. Analogously, bulk particles did not significantly increase their mean size in the presence of serum proteins (BAN = 260 ± 20 nm and BRU = 755 ± 180 nm) compared to deionized water (243 ± 16 nm and 717 ± 55 nm, respectively).

In deionized water, DLS measurements of An-10, RU-10 and BRU are in agreement with CLS data except for the hydrodynamic diameter of BAN. When TiO_2 NPs were diluted in complete culture medium, both Ru-10 and BAN displayed a significantly different hydrodynamic diameter ($p < 0.01$ and $p < 0.001$, respectively) in comparison to the native stock suspensions. Moreover,

CLS analysis showed that at increasing time points the presence of serum did not significantly change the mean size diameter of TiO_2 NPs.

In vitro cytotoxicity of TiO_2 NPs: evaluation of the clonogenic potential

At 24 h exposure, none of the investigated TiO_2 NPs significantly impaired the formation of Balb/3T3 colonies. Compared to deionized water, which was used as C solv (100% CFE ± 3.02), a slight but not significant CFE reduction (Figure 2) was observed in Balb/3T3 cells exposed to 5 µg/ml Ru-10 (95.96% CFE ± 5.99) and to 5 µg/ml and 10 µg/ml BRU (97.17% CFE ± 5.21 and 96.97% CFE ± 2.6, respectively).

In contrast, 72 h exposure of Balb/3T3 cells to Ru-10 and BRU at 5 µg/ml and 10 µg/ml doses significantly reduced the CFE: 5 µg/ml Ru-10 impaired the CFE to 73.7% CFE ± 3.62 and 10 µg/ml Ru-10 to 80.22% CFE ± 4.81. Similarly, 5 µg/ml and 10 µg/ml BRU affected the formation of Balb/3T3 colonies to 78.24% CFE ± 2.78 and to 79.38% CFE ± 3.97, respectively. A non-significant impairment of CFE was observed following 72 h exposure to An-10. In fact, compared to the C solv (100% CFE ± 5.84), 5 µg/ml and 10 µg/ml reduced the scored Balb/3T3 colonies to 92.85% CFE ± 3.38 and to 89.64% CFE ± 7.0, respectively. In addition, a statistically non-significant cytotoxic effect was also observed in the presence of 1 µg/ml Ru-10 (82.21% CFE ± 8.54) and 1 µg/ml BRU (92.0% CFE ± 7.53). Taken together, our results indicated that the crystalline form (rutile) might be responsible for TiO_2 NPs cytotoxicity in Balb/3T3 mouse fibroblasts.

Genotoxicity and morphological neoplastic transformation induced by TiO_2 NPs

Since the concentration of 10 µg/ml resulted sub-toxic or non-toxic for all the tested titania, it was selected as the most suitable concentration for genotoxicity and morphological neoplastic transformation tests. Using CBMN test, we observed that in the presence of TiO_2 NPs, the nuclear division index (NDI; Figure 3A) did not significantly change as compared to C solv (NDI = 2.02) and confirmed that, for each experimental condition, Balb/3T3 cells replicated at least one time during the exposure period, as recommended by the Test Guideline 487 (OECD, 2010). The analysis of micronuclei (MN) induction, as indicator of chromosomal damage, showed that a statistical significant ($p < 0.001$) result in comparison with C solv was observed only after exposure to 10 µg/ml Ru-10 and to the positive control 0.15 µg/ml MMC (Figure 3B). We further investigated the morphological neoplastic transformation potential of TiO_2 NPs by performing the *in vitro* cell transformation assay (Figure 4). Compared to C solv (Tf = 1.4×10^{-4} ± 0.1) Ru-10 induced statistically significant dose-dependent increasing transformation frequency. Similarly, BRU resulted transforming Balb/3T3 cells, and the highest Tf was scored at the highest tested dose (3.8×10^{-4} ± 0.2 at 10 µg/ml). Although An-10 and BAN slightly enhanced type-III foci formation, their effect was not statistically significant.

TiO_2 NPs – Balb/3T3 interaction: uptake quantification

Balb/3T3 were exposed to treatment suspensions at the theoretical concentration of 0.5 mg/ml for 72 h and in order to quantify the real titanium concentration, the treatment suspensions were analysed by ICP-MS. As shown in Figure 5A, Ru-10 (real concentration 0.51 ± 0.01 mg/ml) seems to be the most consistent with the expected theorical concentration; the measured An-10 and BAN (0.55 ± 0.01 mg/ml and 0.44 ± 0.01 mg/ml, respectively) were slightly different from the theorical concentration, but the difference was not statistically significant. BRU, in contrast,

appeared as the treatment suspension that more significantly ($p < 0.001$) differed from the theoretical concentration (0.71 ± 0.02 mg/ml versus 0.5 mg/ml expected). This behaviour was probably due to the higher size distribution and higher tendency to aggregate as compared to the other titania tested (Table 1, 2).

Interestingly, when the number of TiO_2 NPs uptaken per cell was calculated (Figure 5B), nanosized anatase and rutile titania were internalized more significantly ($p < 0.001$) compared to their bulk counterparts: An-10 resulted being the most uptaken nanoparticles ($1.07x10^8$ ± $2.56x10^6$ NPs), followed by Ru-10 ($1.93x10^7$ ± $1.44x10^6$ NPs), BAN ($3.26x10^5$ ± $6.6x10^3$ NPs) and BRU ($7.14x10^4$ ± $5.3x10^3$ NPs). Additionally, the number of anatase TiO_2 NPs, either in the nanorange or in the bulk form, was statistically significant ($p < 0.001$) compared to rutile.

Coherently, the quantification of the amount of Ti, expressed as pg/ml, still present in the collected supernatant at the end of the exposure period (Figure 5C) showed that BAN and BRU contained more Ti (5246.17 ± 114.03 pg/ml and 5895.15 ± 110 pg/ml, respectively) as compared to An-10 (299.68 ± 27 pg/ml) and Ru-10 (1291.48 ± 63 pg/ml). Consistently, the amount of Ti (pg/cell) internalized by Balb/3T3 mouse fibroblasts (Figure 5D) was higher in Ru-10 and An-10 (5.06 ± 0.1 pg/cell and 4.15 ± 0.1 pg/cell, respectively) than in BAN (0.69 ± 0.1 pg/cell) and BRU (0.52 ± 0.06 pg/cell).

Taken together, the uptake quantification data showed a correlation with the hydrodynamic diameter of the particles with a size-dependent pattern. The nanosized titania, which displayed the lower hydrodynamic diameter as shown in Table 2, were more easily internalized by Balb/3T3 than their respective bulks, indicating that size plays a role in the process.

Interestingly, although An-10 was uptaken by Balb/3T3 mouse fibroblasts as efficiently as Ru-10, the internalization of the particles did not correlate with the toxicity data, which showed

indeed a slightly more significant effect in the presence of nano-rutile titania, thus suggesting that the toxicity is triggered by the crystalline form of TiO_2 NPs.

Discussion

Although TiO_2 NPs are currently used in numerous industrial applications, a careful evaluation of their toxic potential is still needed. In this context, we studied the potential cytogenotoxicity, morphological neoplastic transformation and internalization of TiO_2 NPs, and we showed that their crystalline form is a key parameter in their toxicity effect in Balb/3T3 fibroblasts. By colony forming efficiency assay, under our experimental conditions, cytotoxicity was not observed at 24 h exposure in the presence of titania, whereas at 72 h incubation 5 and 10 µg/ml nanosized and bulk rutile titania significantly affected the formation of Balb/3T3 colonies. Similar effects are already reported in the literature (Table 3). Sweeney and co-authors (2014) reported that the membrane integrity of TT1 human alveolar type-I-like epithelial cells was not affected by nanosized anatase and rutile titania, the same that was used in the present study. In contrast, Ru-10 seemed to have a greater pro-inflammatory activity because it stimulated a higher IL-6 and MCP-1 secretion compared to An-10 (Sweeney *et al*. 2014). At 1 – 5 – 10 µg/ml by MTT assay, Saquib and co-authors (2012) demonstrated that rutile TiO_2 NPs impaired the viability of WISH human amnion cells, and the toxicity at 24 h was comparable to our CFE results at 72 h. These different results can be explained taking into consideration the size of the particles: while Saquib *et al*. (2012) studied TiO_2 NPs with hydrodynamic diameter of 30 nm, our rutile titania ranged from 60 - 80 nm (Ru-10) to 730 - 750 nm (BRU) and that could have deferred the cytotoxic effect.

Our results show that the cytotoxicity of TiO_2 NPs might not be simply triggered by the size of the particles, but that the crystalline form plays a role as well. In fact, while we measured a significantly higher internalization of anatase TiO_2 NPs, it was the rutile crystalline form that induced cytotoxicity, genotoxicity and morphological transformation in Balb/3T3 fibroblasts. This effect was already reported in V79 cells, where within 24 h rutile TiO_2 nanorods (420 nm) reduced the cell survival more severely than 365 - 460 nm anatase ones (Hamzeh and Sunahara, 2013). Nevertheless, size-related cytotoxic effects exerted by rutile TiO_2 NPs in normal human skin fibroblasts, in Chinese hamster ovary and in rat basophilic leukemia cells were also reported. As shown by Uchino *et al*. (2011), 20 nm rutile titania resulted more cytotoxic than 250 nm ones, and the effect positively correlated with the amount of particles internalized. Similarly, by ICP-MS we also detected a more significant internalization of nano-rutile TiO_2 NPs compared to its bulk, which could explain the higher toxicity induced by Ru-10 compared to BRU.

Under our experimental conditions, we showed that Balb/3T3 colony formation is not affected upon exposure to low concentrations (1 - 5 - 10 μg/ml) of bulk and nano-anatase titania. Similarly, Kim *et al*. (2010) reported that, up to 500 μg/ml, anatase TiO_2 NPs were not able to inhibit A549 and L-132 colony formation. Moreover, 15 nm TiO_2 NPs (10 - 100 μg/ml) increased the survival of NIH-3T3 cells as shown by CFE assay (Huang *et al.*, 2009). Taken together these results confirm that the crystalline structure has a key role in the cytotoxicity of TiO_2 NPs.

In contrast, previous studies reported that also anatase titania exert cytotoxic effects (Table 3). Cytotoxicity was detected in A549 cells exposed to anatase TiO_2 NPs; analogously, anatase titania affected the mitochondrial integrity of human-derived glial cells (Huerta-Garcia *et al*. 2014) and V79 hamster lung fibroblasts (Chen *et al*. 2014).

In addition to their cytotoxic potential, TiO_2 NPs were already reported to induce genotoxic effects (Table 3). Anatase TiO_2 NPs of 20 nm slightly enhanced MN formation in binucleated CHO-K1 cells after 24 h treatment (Di Virgilio *et al.*, 2010), and in HaCaT cells 10 μg/ml of 200 nm TiO_2 NPs significantly increased the MN rate (Jaeger *et al*., 2012). Additionally, Shukla *et al*. reported that the dose-dependent increase in MN frequency and the induction of oxidative DNA lesions observed in A431 human epidermal cells were correlated to an enhanced lipid peroxidation following exposure to 170 nm anatase TiO_2 NPs (Shukla *et al.*, 2011). Moreover, Falck and co-authors (2009) showed that anatase TiO_2 NPs (hydrodynamic diameter below 20 nm) enhanced the MN frequency in human derived bronchial cells BEAS-2B.

Our results partially confirmed these data, as we observed MN induction in Balb/3T3 at longer exposure periods (48 h), and only the chromosome aberrations induced by Ru-10 were statistically significant. In contrast, nano-rutile TiO_2 NPs filaments, with primary size 10 x 40 nm, were reported to not increase MN frequency in BEAS-2B cells (Falck *et al*. 2009).

Additionally, we showed that the morphological neoplastic transformation is more related to the crystalline form than to the size of the particles: rutile TiO_2 NPs were able to significantly induce type-III foci formation in Balb/3T3 cells, whereas anatase TiO_2 NPs did not. To our knowledge this is the first *in vitro* study directly highlighting the neoplastic transformation potential of TiO_2 NPs, as previous investigations reported the same effect but via DNA damage analysis and, therefore, via a secondary genotoxic mechanism.

Additionally, we demonstrated that rutile and anatase TiO_2 NPs are internalized by Balb/3T3 cells, showing thus that the reduced colony forming efficiency and the formation of MN and type-III foci were due to a direct interaction between titania and cells. However, while we observed that the cytotoxic and genotoxic potential of TiO_2 NPs can be associated with their

crystalline form, the uptake of TiO_2 NPs seemed to depend on their size. The nanosized An-10 and Ru-10, which by DLS were shown to have a smaller hydrodynamic diameter compared to their bulk counterparts, were significantly more uptaken compared to BAN and BRU. Even if further studies on NPs dosimetry are necessary to better understand kinetics of nanomaterials and to measure the real administrated, delivered and internalized concentrations (Cohen *et al*., 2013; DeLoid *et al*., 2014), our ICP-MS data are in good agreement with previous published results. Aggregates/agglomerates of rutile TiO_2 NPs were observed by TEM in cytoplasmic vesicles in A549 (Auevuriyavit *et al*., 2012) and WISH cells (Saquib *et al*., 2012). Shukla *et al.* (2011) and Hackenberg *et al.* (2010) detected TiO_2 NPs in the nucleus of, respectively, human epidermal cells and human nasal mucosa cells, while in BEAS-2B cells the massive presence of particles in the perinuclear region was associated to an altered gene transcription induced by titania that, consequently, blocked the nuclear pores (Park *et al.*, 2008).

Taken together, our results showed that the crystalline form has a role in toxicity in Balb/3T3 mouse fibroblasts. Rutile titania was slightly more toxic than anatase TiO_2 NPs. These results might be explained taking into account the different reactivity of the two crystalline forms we have investigated. In fact, rutile TiO_2 NPs are more photocatalytic than anatase and consequently, are able to generate higher amounts of oxygenated free radicals on their own surface (Fenoglio *et al*., 2009; Lipovsky *et al*., 2012). Moreover, since the ability of several types of nanoparticles to trigger genotoxic effects has been demonstrated to be linked to their ROS induction (Magdolenova *et al*., 2014), this can explain the results we have obtained by exposing BALB/3T3 mouse fibroblasts to TiO_2 NPs. Nevertheless, other physicochemical properties (such as size, mono/polydispersity or surface charge) might play a synergistic role in the differences existing between the mechanism of toxicity of rutile and anatase.

Results available in the literature are difficult to compare mainly due to different factors that can alter the properties of nanomaterials such as their source, the synthesis protocol used, size, coating of NPs and their behavior in culture media. Therefore, further investigation on cyto-genotoxicity of titania using a methodological approach linked to a systematic physico-chemical characterization is still required.

Funding

The research leading to these results has received funding from the European Union Seventh Framework Programme (FP7/2007-2013) under grant agreement no. 214478 (NanoReTox).

Acknowledgements

The authors would like to acknowledge Dr. Deborah Berhanu for TiO_2 NPs synthesis and Dr. Fabio Franchini for performing ICP-MS analysis.

References

1. Aueviriyavit S, Phummiratch D, Kulthong K, Maniratanachote R. (2012). Titanium dioxide nanoparticles-mediated in vitro cytotoxicity does not induce Hsp70 and Grp78 expression in human bronchial epithelial A549 cells. *Biol. Trace Elem. Res.* **149(1)**, 123-32.

2. Balls M, Clothier R. (2010). A FRAME response to the Draft Report on Alternative (Non-animal) Methods for Cosmetics Testing: Current Status and Future Prospects--2010. *Altern Lab Anim*. **38(5)**, 345-53.

3. Bernier MC, El Kirat K, Besse M, Morandat S, Vayssade M. (2012). Preosteoblasts and fibroblasts respond differently to anatase titanium dioxide nanoparticles: a cytotoxicity and inflammation study. *Colloids Surf. B Biointerfaces.* **90**, 68-74.

4. Cassaignon S, Koelsch M, Jolivet JP. (2007). From $TiCl_3$ to TiO_2 nanoparticles (anatase, brookite and rutile): thermohydrolysis and oxidation in aqueous medium. *J. Phys. Chem. Solids*. **68(5-6)**, 695-700.

5. Chen Z, Wang Y, Ba T, Li Y, Pu J, Chen T, Song Y, Gu Y, Qian Q, Yang J, Jia G. (2014). Genotoxic evaluation of titanium dioxide nanoparticles in vivo and in vitro. *Toxicol Lett.* **226(3),** 314-319.

6. Chong MN, Jin B, Chow CW, Saint C. (2010). Recent developments in photocatalytic water treatment technology: a review. *Water Res.* **44(10)**, 2997-3027.

7. Cohen J1, Deloid G, Pyrgiotakis G, Demokritou P. (2013). Interactions of engineered nanomaterials in physiological media and implications for in vitro dosimetry. *Nanotoxicology* **7(4)**, 417-31.

8. DeLoid G, Cohen JM, Darrah T, Derk R, Rojanasakul L, Pyrgiotakis G, Wohlleben W, Demokritou P. (2014). Estimating the effective density of engineered nanomaterials for in vitro dosimetry. *Nature Communications.* **5(3514)**, 1-10.

9. Di Virgilio AL, Reigosa M, Arnal PM, Fernández Lorenzo de Mele M. (2010). Comparative study of the cytotoxic and genotoxic effects of titanium oxide and aluminium oxide nanoparticles in Chinese hamster ovary (CHO-K1) cells. *J Hazard Mater*. **177(1-3)**, 711-8.

10. Di Virgilio AL, Reigosa M, de Mele MF. (2010b). Response of UMR 106 cells exposed to titanium dioxide and aluminum oxide nanoparticles. *J. Biomed. Mater. Res. A.* **92(1)**, 80-6.

11. EURL ECVAM RECOMMENDATION (2012). EURL ECVAM recommendation of 14.03.2012 on three Cell Transformation Assays (CTA) using Syrian Hamster Embryo Cells (SHE) and the BALB/c 3T3 mouse fibroblast cell line for *in vitro* carcinogenicity testing.

12. Falck GC, Lindberg HK, Suhonen S, Vippola M, Vanhala E, Catalán J, Savolainen K, Norppa H. (2009). Genotoxic effects of nanosized and fine TiO2. *Hum Exp Toxicol*. **28**, 339-52.

13. Fenoglio I, Greco G, Livraghi S, Fubini B. (2009). Non-UV-induced radical reactions at the surface of TiO2 nanoparticles that may trigger toxic responses. *Chemistry*. **15(18)**, 4614-21.

14. Hackenberg S, Friehs G, Froelich K, Ginzkey C, Koehler C, Scherzed A, Burghartz M, Hagen R, Kleinsasser N. (2010). Intracellular distribution, geno- and cytotoxic effects of nanosized titanium dioxide particles in the anatase crystal phase on human nasal mucosa cells. *Toxicol. Lett.* **195(1)**, 9-14.

15. Hackenberg S, Friehs G, Kessler M, Froelich K, Ginzkey C, Koehler C, Scherzed A, Burghartz M, Kleinsasser N. (2011). Nanosized titanium dioxide particles do not induce DNA damage in human peripheral blood lymphocytes. *Environ. Mol. Mutagen.* **52(4)**, 264-8.

16. Hamzeh M and Sunahara GI. (2013). In vitro cytotoxicity and genotoxicity studies of titanium dioxide TiO2 nanoparticles in Chinese hamster lung fibroblast cells. *Toxicol. In Vitro* **27(2)**, 864-873.

17. Howarter JA and Youngblood JP. (2008). Self-cleaning and next generation anti-fog surfaces and coatings. *Macromol. Rapid Comm.* **29(6)**, 455-466.

18. Huang S, Chueh PJ, Lin YW, Shih TS, Chuang SM. (2009). Disturbed mitotic progression and genome segregation are involved in cell transformation mediated by nano-TiO2 long-term exposure. *Toxicol. Appl. Pharmacol.* **241(2)**, 182-94.

19. Huang L, Chen K, Lin C, Yang R, Gerhardt RA. (2011). Fabrication and characterization of superhydrophobic high opacity paper with titanium dioxide nanoparticles. *J. Mater. Sci*. **46**, 2600-2605.

20. Huerta-García E, Pérez-Arizti JA, Márquez-Ramírez SG, Delgado-Buenrostro NL, Chirino YI, Iglesias GG, López-Marure R. (2014). Titanium dioxide nanoparticles induce strong oxidative stress and mitochondrial damage in glial cells. *Free Radic Biol Med.* **73**, 84-94.

21. IARC/NCI/EPA Working group. (1985). Cellular and molecular mechanisms of cell transformation and standardization of transformation assays of established cell lines for the prediction of carcinogenic chemicals: overview and recommended protocols. *Cancer research* **45**, 2395-2399.

22. IARC (2010). Carbon black, titanium dioxide, and talc. *IARC Monographs on the Evaluation of Carcinogenic Risks to Humans.* **93**, 1-413.

23. Isfort RJ, LeBoeuf RA. (1996). Application of in vitro cell transformation assays to predict the carcinogenic potential of chemicals. *Mutat Res*. **365(1-3)**, 161-73.

24. Jaeger A, Weiss DG, Jonas L, Kriehuber R. (2012). Oxidative stress-induced cytotoxic and genotoxic effects of nano-sized titanium dioxide particles in human HaCaT keratinocytes. *Toxicology* **296(1-3)**, 27-36.

25. Kerckaert GA, LeBoeuf RA, Isfort RJ. (1996). Use of the Syrian hamster embryo cell transformation assay for determining the carcinogenic potential of heavy metal compounds. *Fundam Appl Toxicol*. **34(1)**, 67-72.

26. Kim IS, Baek M, Choi SJ. (2010). Comparative cytotoxicity of Al2O3, CeO2, TiO2 and ZnO nanoparticles to human lung cells. *J. Nanosci. Nanotechnol.* **10(5)**, 3453-8.

27. Kurzepa H, Kyriazis AP, Lang DR. (1984). Growth characteristics of tumors induced by transplantation into athymic mice of BALB/3T3 cells transformed in vitro by residue organics from drinking water. *J Environ Pathol Toxicol Oncol*. **5(4-5)**, 131-8.

28. Lipovsky A, Levitski L, Tzitrinovich Z, Gedanken A, Lubart R. (2012). The different behavior of rutile and anatase nanoparticles in forming oxy radicals upon illumination with visible light: an EPR study. *Photochem Photobiol*. **88(1)**, 14-20.

29. Magdolenova Z, Collins A, Kumar A, Dhawan A, Stone V, Dusinska M. (2014). Mechanisms of genotoxicity. A review of in vitro and in vivo studies with engineered nanoparticles. *Nanotoxicology*. **8(3)**, 233-78.

30. Mohr U, Ernst H, Roller M, Pott F. (2006). Pulmonary tumor types induced in Wistar rats of the so-called "19-dust study". *Exp Toxicol Pathol*. **58(1)**, 13-20.

31. OECD. (2010). Test Guideline No. 487: In Vitro Mammalian Cell Micronucleus Test. OECD Guidelines for the Testing of Chemicals, Section 4, Health Effects. OECD Publishing, Paris. doi: 10.1787/20745788.

32. Park EJ, Yi J, Chung KH, Ryu DY, Choi J, Park K. (2008). Oxidative stress and apoptosis induced by titanium dioxide nanoparticles in cultured BEAS-2B cells. *Toxicol. Lett.* **180(3)**, 222-9.

33. Ponti J, Broggi F, Mariani V, De Marzi L, Colognato R, Marmorato P, Gioria S, Gilliland D, Pascual Garcìa C, Meschini S, Stringaro A, Molinari A, Rauscher H, Rossi F. (2013). Morphological transformation induced by multiwall carbon nanotubes on Balb/3T3 cell model as an in vitro end point of carcinogenic potential. *Nanotoxicology* **7(2)**, 221-33.

34. Saffiotti U, Ahmed N. (1995). Neoplastic transformation by quartz in the BALB/3T3/A31-1-1 cell line and the effects of associated minerals. *Teratog Carcinog Mutagen*. **15(6)**, 339-56.

35. Saquib Q, Al-Khedhairy AA, Siddiqui MA, Abou-Tarboush FM, Azam A, Musarrat J. (2012). Titanium dioxide nanoparticles induced cytotoxicity, oxidative stress and DNA damage in human amnion epithelial (WISH) cells. *Toxicol. In Vitro* **26(2)**, 351-361.

36. Shi H, Magaye R, Castranova V, Zhao J. (2013). Titanium dioxide nanoparticles: a review of current toxicological data. *Part Fibre Toxicol*. **10**, 15.

37. Shukla RK, Sharma V, Pandey AK, Singh S, Sultana S, Dhawan A. (2011). ROS-mediated genotoxicity induced by titanium dioxide nanoparticles in human epidermal cells. *Toxicol. In Vitro* **25(1)**, 231-41.

38. Sweeney S, Berhanu D, Ruenraroengsak P, Thorley AJ, Valsami-Jones E, Tetley TD. (2014). Nano-titanium dioxide bioreactivity with human alveolar type-I-like epithelial cells: Investigating crystalline phase as a critical determinant. *Nanotoxicology*. 2014 Aug 19:1-11. [Epub ahead of print].

39. Uboldi C, Giudetti G, Broggi F, Gilliland D, Ponti J, Rossi F. (2012). Amorphous silica nanoparticles do not induce cytotoxicity, cell transformation or genotoxicity in Balb/3T3 mouse fibroblasts. *Mutat. Res*. **745(1-2)**, 11-20.

40. Uchino T, Ikarashi Y, Nishimura T. (2011). Effects of coating materials and size of titanium dioxide particles on their cytotoxicity and penetration into the cellular membrane. *J. Toxicol. Sci.* **36(1)**, 95-100.

41. Valsami-Jones E, Berhanu D, Dybowska A, Misra S, Boccaccini AR, Tetley TD, Luoma SN, Plant JA. (2008). Nanomaterial synthesis and characterization for toxicological studies: TiO2 case study. *Mineralogical Magazine*. **72(1)**, 515-519.

42. Vanparys P, Corvi R, Aardema MJ, Gribaldo L, Hayashi M, Hoffmann S, Schechtman L. (2012). Application of in vitro cell transformation assays in regulatory toxicology for pharmaceuticals, chemicals, food products and cosmetics. *Mutat Res*. **744(1)**, 111-6.

43. Xu J, Futakuchi M, Iigo M, Fukamachi K, Alexander DB, Shimizu H, Sakai Y, Tamano S, Furukawa F, Uchino T, Tokunaga H, Nishimura T, Hirose A, Kanno J, Tsuda H. (2010). Involvement of macrophage inflammatory protein 1alpha (MIP1alpha) in promotion of rat lung and mammary carcinogenic activity of nanoscale titanium dioxide particles administered by intra-pulmonary spraying. *Carcinogenesis* **31(5)**, 927-35.

44. Weir A, Westerhoff P, Fabricius L, Hristovski K, von Goetz N. (2012). Titanium dioxide nanoparticles in food and personal care products. *Environ. Sci. Technol.* **46**, 2242−2250.

45. Wolf R, Matz H, Orion E, Lipozencić J. (2003). Sunscreens–the ultimate cosmetic. *Acta Dermatovenerol Croat.* **11**, 158–162.

Figure legend

Figure 1. TiO_2 NPs stock suspensions shape and size determination. TEM micrographs of the as-synthesized TiO_2 NPs indicated that An-10 (A) is composed by egg-shaped particles of 11 - 18 nm, while Ru-10 (B) is more elongated and the particles have a mean size diameter of 10 - 35 nm. BAN (C) and BRU (D) were highly aggregated and composed of particles with different geometry.

Figure 2. Cytotoxicity induced by TiO_2 NPs in Balb/3T3 mouse fibroblasts. Colony Forming Efficiency (CFE) was performed on Balb/3T3 cells exposed for 24 h and 72 h to increasing concentrations (1 – 5 – 10 µg/ml) of TiO_2 NPs. Cytotoxicity was not observed after 24 h exposure, while at 72 h 5 µg/ml and 10 µg/ml Ru-10 and BRU significantly impaired the formation of Balb/3T3 colonies. An-10 and BAN did not exert any cytotoxic effect even after 72 h incubation. The positive control sodium chromate (1000 µM) induced complete cell death (0% CFE). Mean of 3 independent experiments including 3 replicates each ± SEM. Data were compared to C solv (deionized water, 100% CFE) and evaluated by *one-way ANOVA* with Bonferroni post hoc analysis. ** $p < 0.01$.

Figure 3. **Genotoxic potential of TiO_2 NPs by CBMN assay.** The Nuclear Division Index (A) demonstrated that cells have divided at least one time during exposure to TiO_2 NPs (24 h exposure with 10 µg/ml titania). The number of binucleated micronucleated cells (BNMN) scored in 1000 binucleated cells containing one of more micronuclei (B) indicated that An-10, Ru-10 and BRU induced MN formation, but only Ru-10 was statistically significant. The

statistical significance was evaluated by *one-way ANOVA* with Bonferroni post hoc analysis in respect to C solv. Mean of 3 independent experiments and 3 replicates each ± SEM. Mitomycin C (0.1 µg/ml) was used as positive control (C+). *** $p < 0.001$.

Figure 4. Morphological neoplastic transformation induced by TiO_2 NPs in Balb/3T3 mouse fibroblasts. All the investigated TiO_2 NPs induced type-III foci formation and the data are expressed as transformation frequency (Tf). Tf was slightly more severe and statistically significant in the presence of Ru-10 and BRU compared to their anatase counterparts. The statistical significance was evaluated by F-Fisher exact test and compared to C solv. Mean of 3 independent experiments including 5 replicates each ± SEM. 3-Methylcholanthrene (4 µg/ml) was used as positive control (C+). * $p < 0.05$; ** $p < 0.01$; *** $p < 0.001$.

Figure 5. TiO_2 NPs – cell interaction: quantification by ICP-MS. Compared to the theorical (0.5 mg/ml), the measured concentration of TiO_2 NPs in the treatment suspensions (A) was significantly different only in BRU (*** $p < 0.001$). Based on the real concentrations measured, the number of TiO_2 NPs uptaken in each cell was calculated (B) and showed that An-10 and Ru-10 were internalized more efficiently (*** $p < 0.001$) than BAN and BRU; moreover, the number of An-10 TiO_2 NPs uptake per Balb/3T3 cell was significantly higher than Ru 10 ($^{###}$ $p < 0.001$) and BAN particles were taken up more (§§§ $p < 0.001$) than BRU. Accordingly, the ICP-MS quantification of the amount of Ti, expressed as pg/ml, in the collected supernatant (C) revealed that bulk materials and the rutiles were the less internalized titania (*** $p < 0.001$). The quantification of the amount of Ti (pg/cell) uptaken by the total amount of Balb/3T3 mouse fibroblasts (D) after 72 h exposure showed that nanosized TiO_2 NPs were internalized more (***

$p < 0.001$) than bulk, but interestingly showed that Ti from Ru-10 was significantly higher ($^{\#}p < 0.05$) than An-10. Mean of 2 independent experiments ± SEM.

Tables

Table 1. Characterization of TiO_2 NPs by Dynamic Light Scattering. The hydrodynamic diameter and the Z-potential at pH 7 were measured for TiO_2 NPs stock suspensions diluted in deionized water.

Sample name	**Hydrodynamic diameter (nm)**	**PDI [a]**	**Z-pot (mV) at pH 7.0**
An-10	51.42 ± 0.35	0.24 ± 0.04	- 5.64 ± 0.77
BAN	333.80 ± 2.90	0.19 ± 0.02	- 48.40 ± 1.04
Ru-10	134.40 ± 1.02	0.17 ± 0.01	+ 0.04 ± 0.13
BRU	734.20 ± 15.56	0.24 ± 0.03	- 6.62 ± 3.90

a) polydispersity index

Table 2. CLS disc centrifuge characterization of TiO_2 NPs. The mean size diameter was determined in deionized water (A) and in complete cell culture medium (B) at the concentration of 100 µg TiO_2 NPs / ml; Nominal density for An-10 is 3.89 g/cm^3 and for Ru-10 is 4.23 g/cm^3.

A

Deionized water

t = 0 h	**Hydrodynamic diameter (nm)**		
An -10	49 ± 21	*Ru-10*	61 ± 44
BAN	243 ± 16	*BRU*	717 ± 55

B

Complete cell culture medium

	t (h)	**Hydrodynamic diameter (nm)**		**t (h)**	**Hydrodynamic diameter (nm)**
An-10	0	26 ± 15	*Ru-10*	0	82 ± 8
	24	69 ± 24		24	58 ± 23
	48	65 ± 22		48	63 ± 22
	72	64 ± 21		72	60 ± 27
BAN	0	260 ± 20	*BRU*	0	755 ± 180
	24	254 ± 26		24	734 ± N/A
	48	257 ± 22		48	745 ± N/A
	72	260 ± 26		72	766 ± N/A

N/A: not acquirable

Table 3. Toxicological effects of Anatase and Rutile in different sizes as reported in the literature.

Cell Line	Crystalline Structure and Size	Effects observed	Reference
RBL-2H3 rat basophilic leukemia cells	Rutile 20 nm and 250 nm	Size-related cytotoxicity	Uchino et al., 2011
CHO Chinese hamster ovary cells	Rutile 20 nm and 250 nm	Size-related cytotoxicity	Uchino et al., 2011
V79 chinese hamster lung fibroblasts	Anatase 360 - 460 nm Rutile 420 nm	Rutile induced more cytotoxicity (decreased cell viability at concentrations ≥ 10 μg/ml) and apoptosis than anatase; anatase 460 nm was the most genotoxic	Hamzeh & Sunahara, 2013
	Anatase 75 nm	Time- and concentration-dependent impairment of cell viability; genotoxicity was detected at concentrations ≥ 100 μg/ml	Chen et al., 2014
RAW 264.7 mouse macrophage cell line	Rutile 30 - 40 nm	Dose-dependent cytotoxicity and pro-inflammatory activity	Palomaki et al., 2010
bmDC murine bone marrow-derived dendritic cells	Rutile 30 - 40 nm	Dose-dependent cytotoxicity and pro-inflammatory activity	Palomaki et al., 2010
MC-3T3 murine pre-osteoblasts	Anatase 200 - 400 nm	Dose-related cytotoxicity; enhanced IL-6 secretion at concentrations ≥ 20 μg/ml	Bernier et al., 2012
L929 mouse fibroblasts	Anatase 200 - 400 nm	Dose-related cytotoxicity; enhanced IL-6 secretion at concentrations ≥ 500 μg/ml	Bernier et al., 2012
UMR 106 rat osteosarcoma-derived cells	Anatase 21 nm	Dose-dependent cytotoxicity detected at concentrations ≥ 25 μg/ml	Di Virgilio et al., 2010
CHO-K1 chinese hamster ovary cells	Anatase 21 nm	Dose-dependent cytotoxicity detected at concentrations ≥ 5 μg/ml; slight MN formation	Di Virgilio et al., 2010b
NIH3T3 mouse embryonic fibroblasts	Anatase 15 nm	No cytotoxicity observed	Huang et al., 2009

A549 human alveolar carcinoma cells	Anatase 20 - 40 nm	Low impairment of colony formation up to 500 µg/ml	Kim et al., 2010
	Anatase 499 - 2865 nm Rutile 321 - 4235 nm	Dose-related cytotoxicity and mitochondrial impairment	Auevuriyavit et al., 2012
WISH human amnion epithelial cells	Rutile 30.6 nm (TEM), 13 - 308 nm (DLS)	Dose-dependent impairment in the cell survival	Saquib et al., 2012
HaCaT human keratinocytes	Anatase 200 nm	Significant MN formation after 24-48 h and oxidative stress after 4 h exposure	Jaeger et al., 2012
NHSF normal human skin fibroblasts	Rutile 20 nm and 250 nm	Size-related cytotoxicity	Uchino et al., 2011
U373 human glioblastoma astrocytoma cells	Anatase 420 nm	Induction of oxidative stress and mitochondrial depolarization	Huerta-Garcia et al. 2014
Caco-2 human epithelial colorectal adenocarcinoma cells	Anatase 200 nm	No cytotoxic effects	De Angelis et al., 2013
TT1 human alveolar type-I-like epithelial cells	Anatase 10 - 11 nm Rutile 9 - 12 nm	No cytotoxicity up to 100 µg/ml; dose-related IL-6 release, slightly greater following exposure to rutile	Sweeney et al., 2014
Primary human nasal epithelial cells	Anatase 15 - 30 nm	No cytotoxicity nor genotoxicity detected	Hackenberg et al., 2010
Freshly isolated human peripheral blood lymphocytes	Anatase 15 - 30 nm	No significant reduction of cell viability; no evidence for genotoxicity up to 200 µg/ml	Hackenberg et al., 2011
A431 human epidermal cells	Anatase 125 nm	Concentration and time dependent impairment of cell viability; dose-related DNA damage; significant MN formation	Shukla et al., 2011
BEAS-2B human bronchial epithelial cells	Anatase < 25 nm Rutile fibers 10 x 40 nm	Anatase reduced cell viability more severely than rutile; dose-related MN formation after exposure to rutile	Falck et al., 2009
L132	Anatase 20-40 nm	No impairment of cell viability and of colony	Kim et al., 2010

normal human lung cells	formation

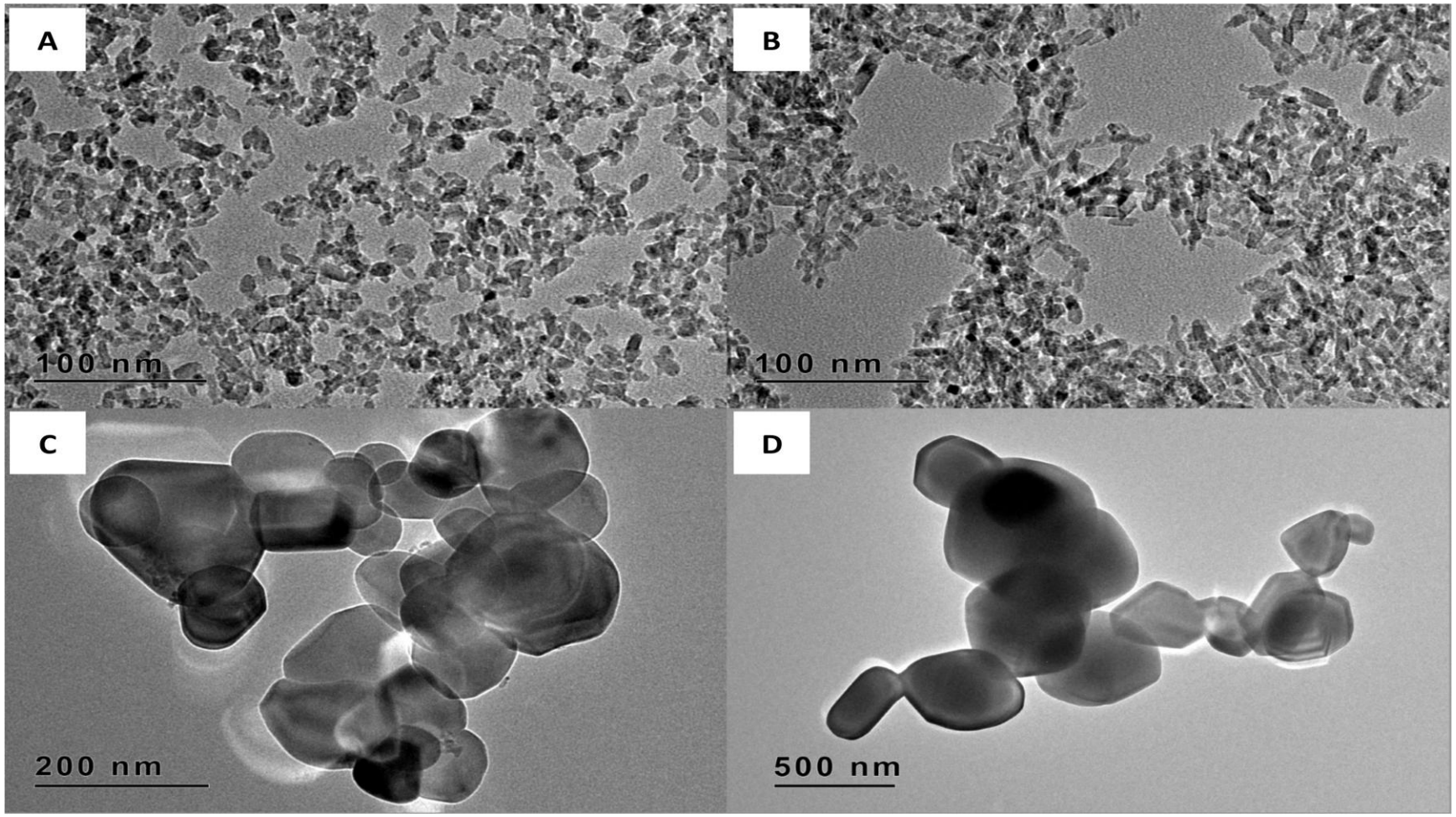

Figure 1

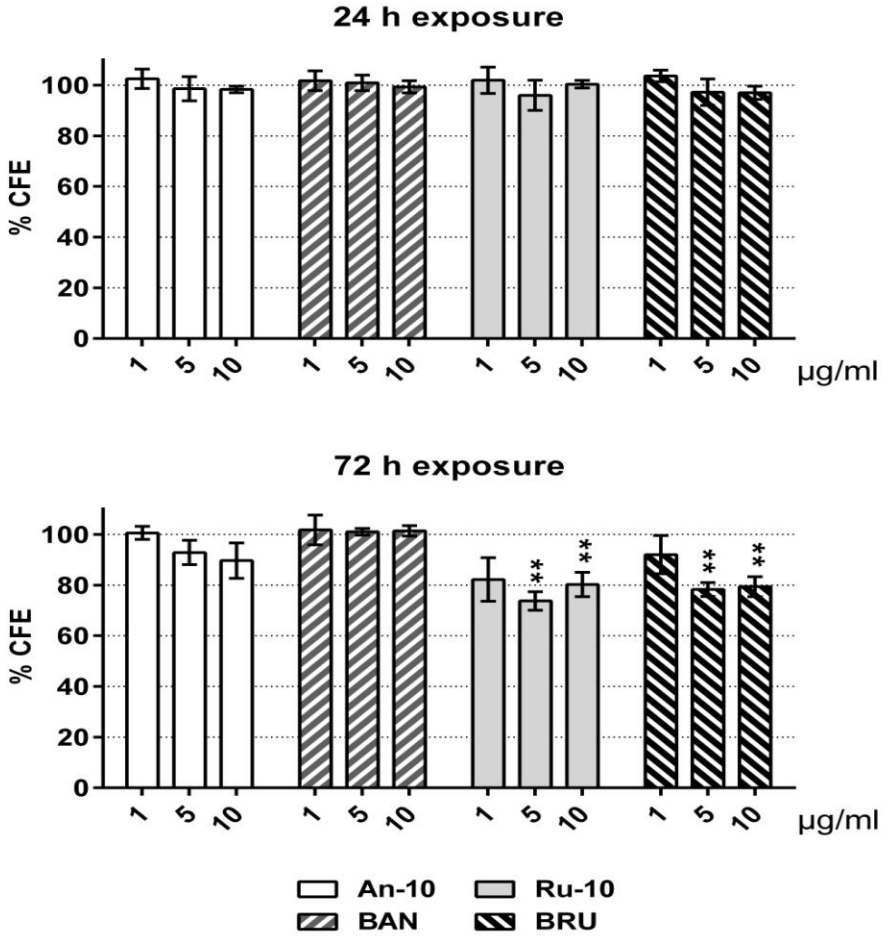
24 h exposure
% CFE
100
80
60
40
20
0
1
5
10
µg/ml
72 h exposure
**
An-10
Ru-10
BAN
BRU

Figure 2

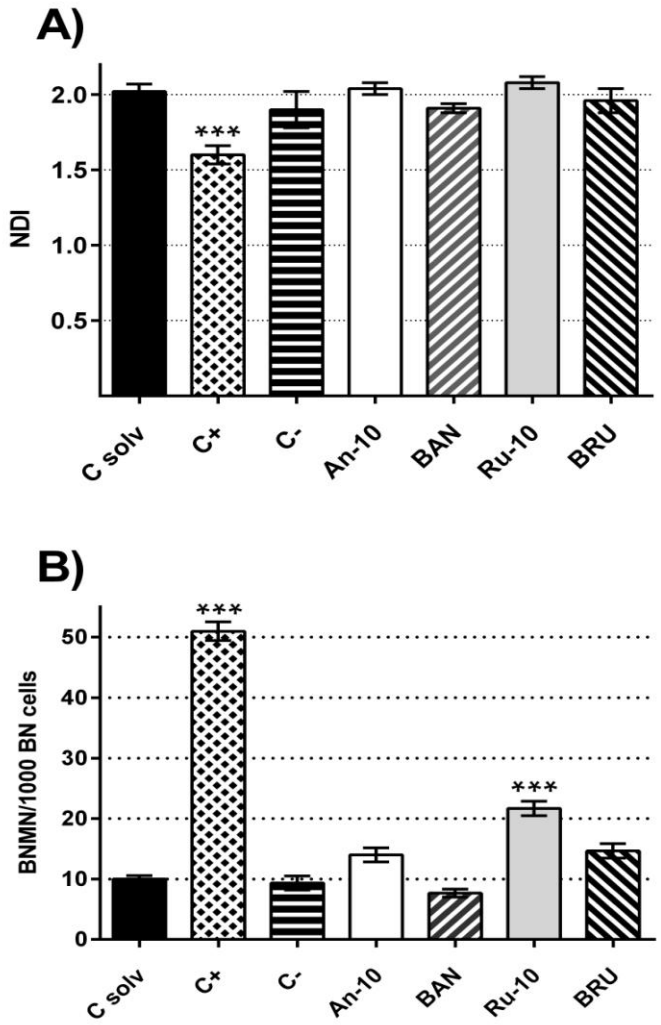
A)
NDI
2.0
1.5
1.0
0.5
***
C solv
C+
C-
An-10
BAN
Ru-10
BRU
B)
BNMN/1000 BN cells
50
40
30
20
10
0
***
***
C solv
C+
C-
An-10
BAN
Ru-10
BRU

Figure 3

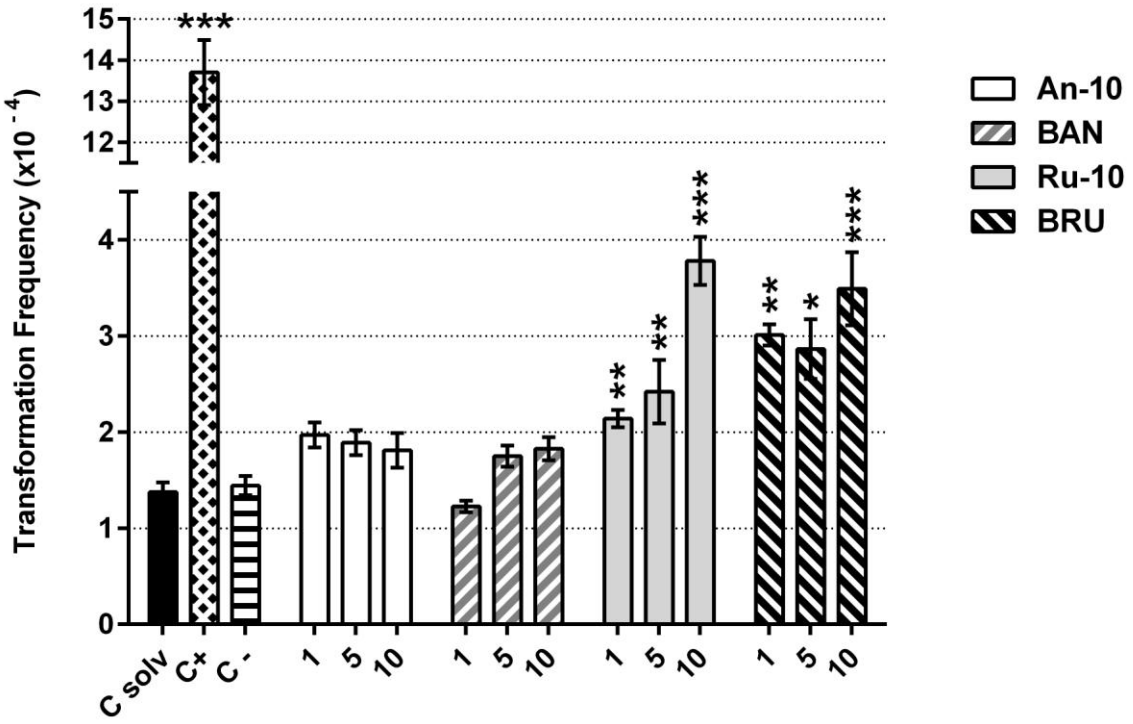
Transformation Frequency (x10 -4)
15
14
13
12
4
3
2
1
0
***
**
**
***
**
*
***
C solv
C+
C -
1
5
10
1
5
10
1
5
10
1
5
10
An-10
BAN
Ru-10
BRU

Figure 4

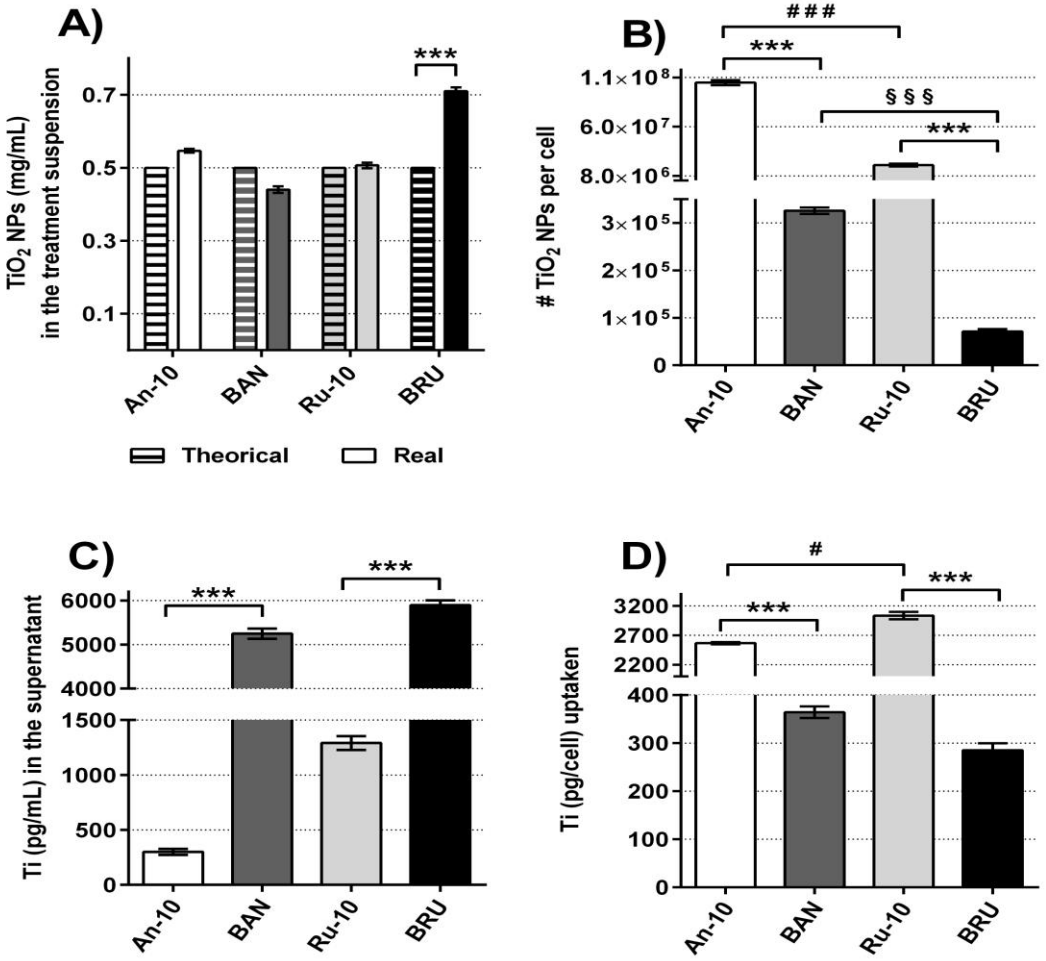
A)
TiO2 NPs (mg/mL) in the treatment suspension
0.7
0.5
0.3
0.1
***
An-10
BAN
Ru-10
BRU
Theorical
Real
B)
TiO2 NPs per cell
1.1×10^8
6.0×10^7
8.0×10^6
3×10^5
2×10^5
1×10^5
0
###
***
§§§
***
C)
Ti (pg/mL) in the supernatant
6000
5000
4000
1500
1000
500
0
***
***
D)
Ti (pg/cell) uptaken
3200
2700
2200
400
300
200
100
0
#
***
***

Figure 5